Artificial quantum confinement in $LaAlO_3/SrTiO_3$ heterostructures

M. Caputo,1,* M. Boselli,2 A. Filippetti,3 S. Lemal,4 D. Li,2 A. Chikina,1,† C. Cancellieri,5 T. Schmitt,1 J.-M. Triscone,2 P. Ghosez,4 S. Gariglio ,2 and V. N. Strocov1

[1]*Swiss Light Source, Paul Scherrer Institute, CH-5232 Villigen, Switzerland*
[2]*Department of Quantum Matter Physics, University of Geneva, CH-1211 Geneva, Switzerland*
[3]*Department of Physics at University of Cagliari, and CNR-IOM, UOS Cagliari, Cittadella Universitaria, I-09042 Monserrato (CA), Italy*
[4]*Theoretical Materials Physics, Q-MAT, CESAM, University of Liège, B-4000 Liège, Belgium*
[5]*Empa, Swiss Federal Laboratories for Materials Science & Technology, Ueberlandstrasse 129, Duebendorf CH-8600, Switzerland*

Heterostructures of transition metal oxides perovskites represent an ideal platform to explore exotic phenom- ena involving the complex interplay between the spin, charge, orbital and lattice degrees of freedom available in these compounds. At the interface between such materials, this interplay can lead to phenomena that are present in none of the original constituents such as the formation of the interfacial two-dimensional electron system (2DES) discovered at the LAO3/STO3 (LAO/STO) interface. In samples prepared by growing a LAO layer onto a STO substrate, the 2DES is confined in a band bending potential well, whose width is set by the interface charge density and the STO dielectric properties, and determines the electronic band structure. Growing LAO (2 nm) /STO (x nm)/LAO (2 nm) heterostructures on STO substrates allows us to control the extension of the confining potential of the top 2DES via the thickness of the STO layer. In such samples, we explore the electronic structure trend under an increase of the confining potential with using soft x-ray angle-resolved photoemission spectroscopy combined with ab initio calculations. The results indicate that varying the thickness of the STO film modifies the quantization of the 3d t2g bands and, interestingly, redistributes the charge between the dxy and dxz/dyz bands.

Advances in thin-film deposition techniques have led to the discovery of a variety of phenomena in artificial heterostructures ranging from the quantum Hall effect to topological states. For epitaxial stacks, perovskites of transition metal oxides are particularly interesting because, sharing a common crystal structure, they display a unique interplay of spin, orbital, charge, and lattice degrees of freedom leading to a wide range of intriguing physical properties such as nonlinear optical response, colossal magnetoresistance, high-temperature superconductivity, etc. [1]. Among several phenomena reported for such heterostructures [2,3], one of the most remarkable observations is the conductivity discovered between two insulating materials. Originally detected at the interface between $LaAlO_3$ (LAO) and $SrTiO_3$ (STO) [4], two wide-gap insulators, it was also observed between $LaTiO_3$, a Mott insulator, and $SrTiO_3$ [5] as well as between $LaTiO_3$ and $KTaO_3$ [6]. The origin of the observed conductivity is possibly related to the occurrence of a polar discontinuity between the two crystals, a common feature of these heterostructures [7,8]. Extensive work on the electronic properties of this interfacial system has shown that the band bending potential at the interface creates a quantum well (QW) that hosts the mobile electron system [9,10]. For interfaces prepared by growing a $LaAlO_3$ layer on top of a $SrTiO_3$ substrate, the vertical extension of the conducting region is found to be around 10 nm at low temperatures [11,12] and such confinement determines the electronic structure of the two-dimensional (2D) electron system (2DES); the t_{2g} bands, degenerate in STO bulk, split into the d_{xy} and d_{xz}/d_{yz} ones as a consequence of the in-plane vs out-of-plane extension of these orbitals [10,13]. Although the polar discontinuity is absent at the bare STO surface, certain treatments, for instance UV illumination, can dope electrons into the t_{2g} manifold of the conduction band [13–15], inducing a metallic surface state that bears similarities to the LAO/STO interface.

The 2DES at the LAO/STO interface was found to be conducting, superconducting, and to display a Rashba-type spin-orbit interaction [8]. With this interface being a quite unique playground, several approaches have been used to manipulate its properties. The most common one is the field effect, particularly efficient due to the low density of the charge carriers, estimated on the order of a few 10^{13} cm^{-2}. Gating allowed, for instance, the tuning of the (super)conducting state [16,17], switching on and off the (zero-resistance) conductance, and the control of the spin-orbit interaction strength [18]. Other approaches have also been used to modify the properties of the 2DES such as variation of the growth conditions, stoichiometry, strain, oxygen deficiency, and absorption of gases on the LAO surface [19–24].

In this paper, we explore an interesting possibility to control the electronic properties of the 2DES. The idea is

*Corresponding author: marco.caputo@psi.ch
†Present address: Department of Physics and Astronomy, Interdisciplinary Nanoscience Center, Aarhus University, 8000 Aarhus C, Denmark.

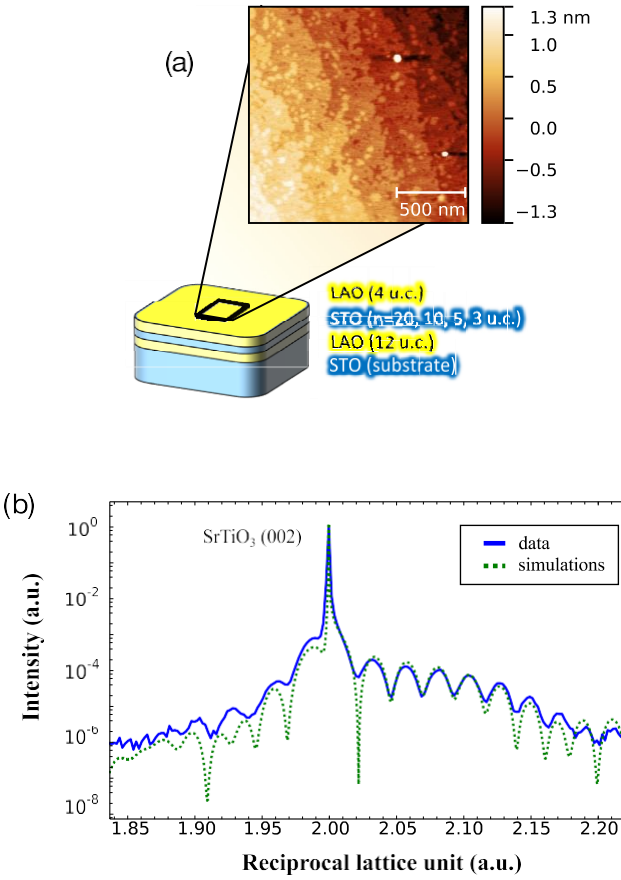

FIG. 1. (a) Scheme of the samples, and an AFM image showing the typical topography of the topmost layer. (b) X-ray diffraction data of an example LAO (10 u.c.)/STO (35 u.c.)/LAO (5 u.c.) sample, showing the 002 reflection of the substrate together with the fringes originated from the ultrathin films. Data are compared with a calculated pattern using the following out-of-plane axis values: c(LAO, 5 u.c.) = 3.773 A, c(STO, 35 u.c.) = 3.91 Å, c(LAO, 10 u.c.) = 3.766 A.

to induce the 2DES in an STO thin film whose thickness can be chosen below the natural extension of the 2DES in standard LAO/STO interfaces. Such an approach results in additional confinement of the 2DES which can modify its electronic structure. To this aim, we have grown a series of LAO/STO/LAO thin film heterostructures on STO substrates to control the extension of the QW potential through the thickness of the STO layer. Resonant angle-resolved photoemission spectroscopy (ARPES) and *ab initio* calculations reveal the evolution of the electronic band structure of the 2DES with the STO layer thickness, uncovering a change in the energy separation and population of the d_{xy} and d_{xz}/d_{yz} bands as well as charge redistribution between them. These effects are driven by quantization of the electron states confined in the STO layer in the presence of electron correlations.

A sketch of the investigated structures is shown in Fig. 1. On a (001)-oriented TiO_2-terminated STO substrate, a first LAO layer of 12 unit cells (u.c.) is grown by pulsed laser deposition. On top of this, we deposit the STO layer hosting the 2DES which is induced by a 4 u.c. LAO layer grown on top (details on the growth and physical properties of these

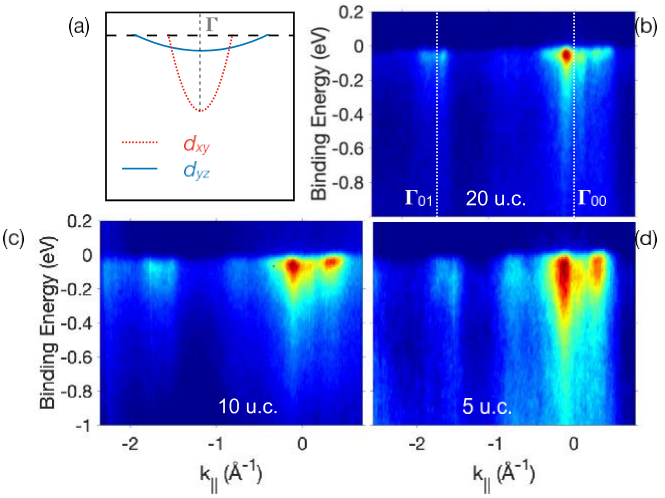

FIG. 2. (a) Shows a schematic of the electronic structure along the Γ-X direction of the 2DES of a "standard" bulk LAO/STO interface. (b)–(d) are the experimental electronic structures for the n = 20, 10, and 5 u.c. samples (marked on the panel).

samples, sensitive to the growth conditions, are provided in the Supplemental Material [25,34]). Such structure creates two conducting interfaces localized in different regions: one at the top LAO film/STO film interface and one at the bottom LAO film /STO substrate interface. However, as explained below, ARPES is mostly probing the top 2DES whose vertical extension is limited by the thickness of the STO layer. The number (n) of unit cells for this STO layer was varied from n = 20, a thickness corresponding to the self-confinement of the electron system that is observed in standard LAO/STO substrate interfaces at low temperature, down to n = 5.

The electronic structure of these samples was investigated using (resonant) soft x-ray angle-resolved photoemission spectroscopy (SX-ARPES) at the ADRESS beamline at SLS [35]. Using soft x-rays photons instead of the commonly used vacuum ultraviolet (VUV) ones, one can overcome the major drawbacks of the ARPES technique, namely, its extreme surface sensitivity. The probing depth of SX-ARPES is indeed higher by a factor of about four with respect to the VUV-ARPES [36], and its yield can be pushed even further using core-hole assisted photoemission processes [37]. Buried interfaces are a natural application field for this technique, and we refer the reader to a recent review for a detailed description [38]. The probing depth of SX-ARPES in our energy range accentuates the signal from the topmost LAO/STO interface, with the signal coming from the deeper second interface being less than 10% of the total for the ultimate limit of 5 u.c. of STO. All the data presented here, if not stated elsewhere, were acquired using a photon energy of 466 eV corresponding to the L_2 absorption edge of Ti: this gives us a clearer photoemission yield for the d_{yz} band compared to the d_{xy} one [37]. Moreover, the choice of *s*- polarized x rays allows us to silence signal coming from the d_{xz} band, due to the symmetry of our experimental geometry [35]. For the simulation of the electronic properties of the heterostructure, we use two beyond-standard methodologies which, correcting the known shortcomings of the standard density functional theory (DFT),

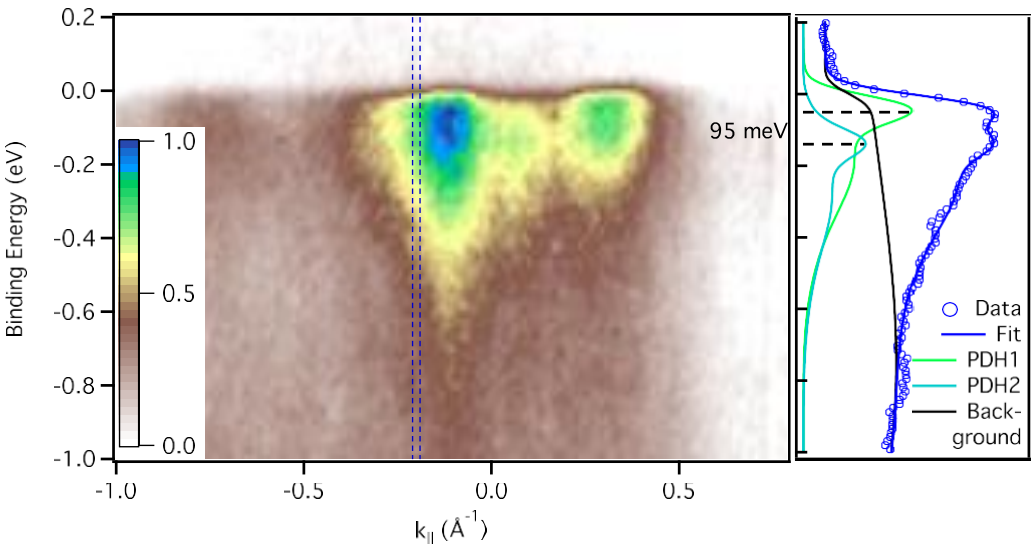

FIG. 3. Detail of the electronic structure (left panel) of the $n=5$ u.c. sample along the Γ-X direction. The blue dashed lines represent the integration window of the EDC (right panel) plotted together with the fitting results. The horizontal dashed lines highlight the double-peak structure (see text for details).

accurately describe strongly-correlated oxides: the variational pseudo-self-interaction corrected (VPSIC) DFT [39,40], and the B1-WC hybrid functional [27,41].

Figure 2 shows experimental SX-ARPES intensity images representing the evolution of the electronic structure of the 2DES at the top LAO/STO interface of samples with a different thickness of the STO embedded layer. All the images are acquired in the same conditions along the Γ-X direction of the Brillouin zone at a temperature of 13 K.

Figure 2(b) ($n=20$ u.c.) reveals an electronic structure very similar to the one of a "standard" LAO/STO interface realized at the TiO_2-terminated (001) STO substrate surface [42,43] [whose scheme is illustrated in Fig. 2(a)]. At the Fermi level, the band structure is dominated by a weakly dispersing band originated from the Ti d_{yz} orbitals, extending through the region $k_{\parallel} \approx 0.39$ Å^{-1}. Superimposed to this heavy band, two bright spots appear at $k_{\parallel} \approx 0.09$ Å^{-1}: these correspond to the points where the band originating from the Ti $d_{yz/xz}$ orbitals hybridizes with the Ti d_{xy}-originated bands. Strong out-of-plane localization of these bands makes its soft X-ray photoemission yield (and so its visibility) lower with respect to the deeper penetrating d_{yz}-derived bands [44]. Due to matrix element effects, the intensity is different between the two Brillouin zones (Γ_{00} and Γ_{01}) and even not symmetric around the Γ_{00} point ($k_{\parallel} = 0$ Å^{-1}), in particular on the right side of Γ where the intensity of the d_{yz} band is enhanced, while on the left side the intensity ratio between d_{yz} and d_{xy} band intensity is reversed.

Comparing these data with the measurements on the $n=10$ sample [Fig. 2(c)], we notice a clear enhancement of the photoemission yield of the d_{yz} band, together with an energy broadening of the spectral structures. Interestingly, a sizeable spectral weight at the Fermi level appears in the region around -0.75 Å^{-1}, which falls on the boundary between the first and second Brillouin zone. We attribute this to an emerging 2×1 reconstruction already observed by Plumb *et al.* [45]: these authors suggest the occurrence of an octahedral tilting causing folding of the bands. Most importantly, the $n=5$ u.c. sample [Fig. 2(d)], shows a remarkably stronger broadening in the energy direction. In the following, we concentrate our discussion on this sample.

In order to analyze in detail the spectral broadening for the $n = 5$ u.c. sample, we plot in Fig. 3 an enlarged view of its electronic structure (left panel), together with an energy distribution curve (EDC) taken at $k_{\parallel} \approx 0.2$ Å^{-1} (right). The EDC (blue circles) clearly shows a double-peak structure in the range 0–0.2 eV of binding energy. The shape of the EDC is reproduced for all parallel momenta in the range -0.4 Å$^{-1} < k_{\parallel} < 0.2$ Å^{-1} and 0.2 Å$^{-1} < k < 0.4$ Å^{-1} as shown in Fig. S1 (see Supplemental Material [25]), while for momenta in the range 0.2 Å$^{-1} < k_{\parallel} < 0.2$ Å^{-1} the presence of the d_{xy} band introduces additional spectral weight that overshadows the double peak feature. The double-peak structure indicates the presence of a replica band, whose origin can be attributed to two phenomena: formation of a polaronic sideband due to enhanced electron-phonon coupling, or the quantization effect on the d_{yz} band generating subband levels.

STO and STO-based interfaces are known to host polaronic charge carriers easily recognizable by a hump in the spectral function located roughly at 90–120 meV higher binding energy with respect to the quasiparticle (QP) peak [43,46,47]. This hump arises from electron coupling with the LO3 vibrational mode of the O cage. The double peak structure identified in our experimental EDC could, in principle, fit this picture, with the two peaks identifying the quasiparticle and its polaronic hump. In order to check this scenario, we fitted the EDC using a Gaussian peak for the QP band, followed by a series of Gaussians representing each of its polaronic replicas (see Supplemental Material and Fig. S3 for details on the fitting procedure [25]). Using just one of these peak-dip-hump (PDH) spectral shapes, it was not possible to fit the EDC's double peak structure. Moreover, we note that whereas

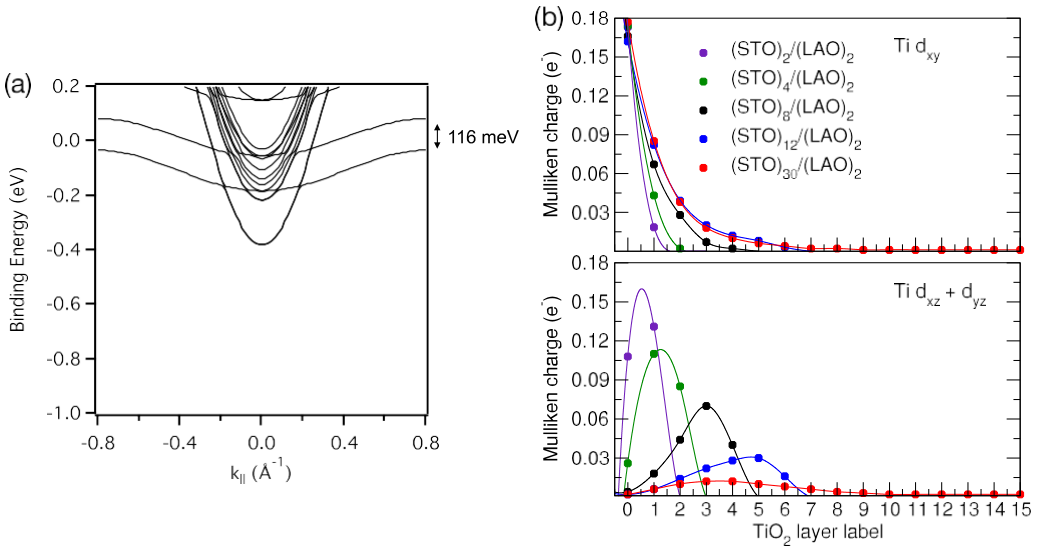

FIG. 4. (a) Band structure calculated for LAO/9.5 u.c. STO slab (see Supplemental Material). (b) Decomposition in the Mulliken scheme electron charge for different 2 u.c. LAO/ n u.c. STO superlattices (n=2, 4, 8, 12, 30, see Supplemental Material) in the different Ti sites. The labeling of the Ti sites starts at 0 for the first TiO_2 next to the LAO plane. Data are interpolated by the mean of cubic splines as a guide to the eye.

all previous studies on the STO-based systems have found that the hump amplitude is significantly smaller compared to the QP peak [43,46,47], in our case the two spectral peaks have similar amplitudes. In contrast, a superposition of two PDH-structures yields a remarkable agreement with the experimental data, as shown in the right panel of Fig. 3. The best fit is achieved for an energy separation between the two PDH curves of 95 $\pm$ 4 meV. A similar fitting procedure has been performed for several EDCs, resulting in a mean energy separation between the two bands of 99 4 meV.

This analysis suggests that what we observe as the second spectral peak is actually a second d_{yz} subband. We attribute the appearance of this band to a modification of the QW potential hosting the 2DES: the confinement of the 2DES in the ultrathin STO embedded layer of the LAO/STO heterostructure lowers the energy of the quantized second d_{yz} subband below the Fermi level. In order to validate this scenario, in Fig. 4(a) we show the band structure calculated by VPSIC for a slab composed of 10 u.c. of STO with 4 u.c. of LAO layers on both STO sides, and a vacuum region equivalent to 3 u.c. LAO above. Since no 2DES has ever been observed when growing STO on LAO, presumably the bottom STO/LAO interface embeds a more shallow potential, making our calculation eventually a good approximation of the potential in two symmetric LAO/5 u.c STO interfaces. The calculations show two d_{yz} bands separated by 116 meV, which is in good agreement with the experimental splitting reported in Fig. 3. Note that the theoretical Fermi level position here is assigned by comparing calculations with the experimental bandwidth: in this case, the first QW state resides completely below the Fermi level; this occurrence has already been observed by Wang *et al.* for the n=1 QW state in anatase TiO_2 [48], making this scenario plausible.

Calculations with the B1-WC energy functional considering a surface charge density of 0.5 e-/u.c. (i.e. the band filling sets the Fermi level self-consistently) confirm the shift of the d_{yz} band to lower binding energy for ultrathin STO layers. Figure 4(b) shows the Mulliken charges on each TiO_2 layer for STO slabs of different thickness, comparing the behavior of d_{xy} orbital states (top graph) with that of $d_{xz/yz}$ states (bottom graph). When the STO thickness is reduced, one can see, both in the top (d_{xy} states) and in the bottom ($d_{xz/yz}$ states) plots, a progressive shift of the charge toward the interface, a natural effect of the thinning of the STO layer. More interesting, by comparing the two graphs, calculations predict a charge transfer from the d_{xy} to the $d_{xz/yz}$ states along with the decrease of the STO thickness: in the ultrathin limit, the amount of charge accumulated in the two bands becomes nearly equal. This finding supports the idea that in the narrow STO slab limit a consistent fraction of charge can also populate the n 2 QW-state with the $d_{xz/yz}$ orbital character. This behavior can be attributed to two effects: on one hand, reducing the QW width increases the energy splitting between subbands of same symmetry, whereas, on the other hand, as the charge accumulates closer to the interface, the occupancy of the d_{xz}/d_{yz} states, localized farther from the interface, is favored because their energies are lowered due to static correlation effects [49–51]. These effects, resembling Hubbard's U , are included into the exchange-correlation potential of our DFT calculations. These results indicate that a combination of quantum confinement with electron correlations, controlled by the thickness of the embedded STO layer, can shift the Fermi level of the 2DES and thereby give a control of the charge carrier density.

A consequence of the reduction of the QW width is the increase of the energy band splitting, appearing in the electronic structures presented in Fig. S5 (see the Supplemental Material [25]). Observing such a trend experimentally is, however, difficult due to the lack of energy resolution for the thicker STO layers, where the quantum wells are very close in energy, and because of the smearing of all spectral structures induced by the growing disorder and interfacial

intermixing in heterostructures with ultrathin STO layers. Figure 2(c) illustrates the case $n = 10$, where a broadening of the spectral features in the energy direction is evident, but it is impossible to distinguish separated QW states, while Fig. S4 shows the experimental data for the $n = 3$ sample: one can notice a qualitative agreement with the VPSIC calculations, but the experimental smearing hinders a more quantitative comparison [25].

In conclusion, the growth of artificial LAO/STO heterostructures with an embedded STO layer forms a 2DES with tunable properties. The tunability is achieved by varying the thickness of the STO layer on a single unit cell scale, which controls the confinement of the 2DES, and thus energy position and population of different QW states. In a wider perspective, the out-of-plane confinement at the interface can be complemented by confinement in the lateral direction, in order to obtain conducting channels with desired charge carrier density. This work paves the way for further nanoscale manipulations of 2DESs at surfaces/interfaces of different transition metal oxides.

ACKNOWLEDGMENTS

This work was supported by the Swiss National Science Foundation through Division II and by the European Research Council under the European Union's Seventh Framework Program (FP7/2007-2013)/ERC Grant Agreement No. 319286 (Q-MAC). We thank O. Stephan and her team at LPS, Université Paris Sud, for the STEM measurements of our samples. A.A.F. thanks "Progetti biennali d'Ateneo Finanziati dalla Fondazione di Sardegna 2017" (Project No. F71I17000170002), and Project No. PRIN 2017 "TOPSPIN", funded by Italian Ministry of University and Research. S.L. and P.G. acknowledge support from the MERA.NET project SIOX as well as access to computational resources provided by the Consortium des Equipements de Calcul Intensif (CECI), funded by the F.R.S.-FNRS under the Grant No. 2.5020.11 and the Tier-1 supercomputer of the Fédération Wallonie-Bruxelles funded by the Walloon Region under the Grant No. 1117545. A.C. work was partially found by the VILLUM FONDEN through the Centre of Excellence for Dirac Materials (Grant No. 11744).

[1] D. I. Khomskii, *Transition Metal Compounds* (Cambridge University Press, Cambridge, 2014).

[2] P. Zubko, S. Gariglio, M. Gabay, P. Ghosez, and J.-M. Triscone, Interface physics in complex oxide heterostructures, Annu. Rev. Condens. Matter Phys. **2**, 141 (2011).

[3] H. Y. Hwang, Y. Iwasa, M. Kawasaki, B. Keimer, N. Nagaosa, and Y. Tokura, Emergent phenomena at oxide interfaces, Nature Mater. **11**, 103 (2012).

[4] A. Ohtomo and H. Y. Hwang, A high-mobility electron gas at the $LaAlO_3/SrTiO_3$ heterointerface, Nature **427**, 423 (2004).

[5] J. Biscaras, N. Bergeal, A. Kushwaha, T. Wolf, A. Rastogi, R. C. Budhani, and J. Lesueur, Two-dimensional superconductivity at a Mott insulator/band insulator interface $LaTiO_3/SrTiO_3$, Nat. Commun. **1**, 89 (2010).

[6] K. Zou, S. Ismail-Beigi, K. Kisslinger, X. Shen, D. Su, F. J. Walker, and C. H. Ahn, LaTiO3/KTaO3 interfaces: A new two-dimensional electron gas system, APL Mater. **3**, 036104 (2015).

[7] M. L. Reinle-Schmitt, C. Cancellieri, D. Li, D. Fontaine, M. Medarde, E. Pomjakushina, C. W. Schneider, S. Gariglio, P.-M. Ghosez, J. Triscone *et al.*, Tunable conductivity threshold at polar oxide interfaces, Nat. Commun. **3**, 932 (2012).

[8] S. Gariglio, M.-M. Gabay, and J. Triscone, Research update: conductivity and beyond at the $LaAlO_3/SrTiO_3$ interface, APL Mater. **4**, 060701 (2016).

[9] C. Cancellieri, M. L. Reinle-Schmitt, M. Kobayashi, V. N. Strocov, T. Schmitt, P. R. Willmott, S.-M. Gariglio, and J. Triscone, Interface Fermi States of $LaAlO_3/SrTiO_3$ and Related Heterostructures, Phys. Rev. Lett. **110**, 137601 (2013).

[10] M. Sing, G. Berner, K. Goß, A. Müller, A. Ruff, A. Wetscherek, S. Thiel, J. Mannhart, S. A. Pauli, and C. W. Schneider *et al.*, Profiling the Interface Electron Gas of $LaAlO_3/SrTiO_3$ Heterostructures with Hard X-Ray Photoelectron Spectroscopy, Phys. Rev. Lett. **102**, 176805 (2009).

[11] M. Basletic, J.-L. Maurice, C. Carrétéro, G. Herranz, O. Copie, M. Bibes, E. Jacquet, K. Bouzehouane, S. Fusil, and A. Barthélémy, Mapping the spatial distribution of charge carriers in $LaAlO_3/SrTiO_3$ heterostructures, Nat. Mater. **7**, 621 (2008).

[12] N. Reyren, S. Gariglio, A. D. Caviglia, D. Jaccard, T.-M. Schneider, and J. Triscone, Anisotropy of the superconducting transport properties of the $LaAlO_3/SrTiO_3$ interface, App. Phys. Lett. **94**, 112506 (2009).

[13] A. F. Santander-Syro, O. Copie, T. Kondo, F. Fortuna, S. Pailhès, R. Weht, X. G. Qiu, F. Bertran, A. Nicolaou, A. Taleb-Ibrahimi *et al.*, Two-dimensional electron gas with universal subbands at the surface of $SrTiO_3$, Nature **469**, 189 (2011).

[14] W. Meevasana, P. D. C. King, R. H. He, S.-K. Mo, M. Hashimoto, A. Tamai, P. Songsiriritthigul, F. Baumberger, and Z.-X. Shen, Creation and control of a two-dimensional electron liquid at the bare $SrTiO_3$ Surface, Nat. Mater. **10**, 114 (2011).

[15] P. Delugas, V. Fiorentini, A. Mattoni, and A. Filippetti, Intrinsic origin of two-dimensional electron gas at the (001) surface of $SrTiO_3$, Phys. Rev.B **91**, 115315 (2015).

[16] S. Thiel, G. Hammerl, A. Schmehl, C. W. Schneider, and J. Mannhart, Tunable quasi-two-dimensional electron gases in oxide heterostructures, Science **313**, 1942 (2006).

[17] A. D. Caviglia, S. Gariglio, N. Reyren, D. Jaccard, T. Schneider, M. Gabay, S. Thiel, G. Hammerl, J. Mannhart, and J.-M. Triscone, Electric field control of the $LaAlO_3/SrTiO_3$ interface ground state, Nature **456**, 624 (2008).

[18] A. D. Caviglia, M. Gabay, S. Gariglio, N. Reyren, C. Cancellieri, and J.-M. Triscone, Tunable Rashba Spin-Orbit Interaction at Oxide Interfaces, Phys. Rev. Lett. **104**, 126803 (2010).

[19] Y. Xie, Y. Hikita, C. Bell, and H. Y. Hwang, Control of electronic conduction at an oxide heterointerface using surface polar adsorbates, Nat. Commun. **2**, 494 (2011).

[20] K. A. Brown, S. He, D. J. Eichelsdoerfer, M. Huang, I. Levy, H. Lee, S. Ryu, P. Irvin, J. Mendez-Arroyo, C.-B. Eom *et al.*, Giant conductivity switching of $LaAlO_3/SrTiO_3$

heterointerfaces governed by surface protonation, Nat. Commun. **7**, 10681 (2016).

[21] W. Dai, S. Adhikari, A. C. Garcia-Castro, A. H. Romero, H. Lee, J.-W. Lee, S. Ryu, C.-B. Eom, and C. Cen, Tailoring $LaAlO_3/SrTiO_3$ interface metallicity by oxygen surface adsorbates, Nano Lett. **16**, 2739 (2016).

[22] E. Lesne, N. Reyren, D. Doennig, R. Mattana, H. Jaffrès, V. Cros, F. Petroff, F. Choueikani, P. Ohresser, R. Pentcheva *et al.*, Suppression of the critical thickness threshold for conductivity at the $LaAlO_3/SrTiO_3$ interface, Nat. Commun. **5**, 4291 (2014).

[23] P. Scheiderer, F. Pfaff, J. Gabel, M. Kamp, M. Sing, and R. Claessen, Surface-interface coupling in an oxide heterostructure: Impact of adsorbates on $LaAlO_3/SrTiO_3$, Phys. Rev. B **92**, 195422 (2015).

[24] D. C. Vaz, D. Castro Vaz, E. Lesne, A. Sander, H. Naganuma, E. Jacquet, J. Santamaria, A. Barthélémy, and M. Bibes, Tuning up or down the critical thickness in $LaAlO_3/SrTiO_3$ through *in situ* deposition of metal overlayers, Adv. Mater. **29**, 1700486 (2017).

[25] See Supplemental Material at http://link.aps.org/supplemental/10.1103/PhysRevMaterials.4.035001 for details on the sample growth and characterization, and technicalities of calculations and ARPES data treatment, see Refs. [26–33].

[26] P. Delugas, A. Filippetti, V. Fiorentini, D. I. Bilc, D. Fontaine, and P. Ghosez, Spontaneous 2-Dimensional Carrier Confinement at the *N* -Type $SrTiO_3/LaAlO_3$ Interface, Phys. Rev. Lett. **106**, 166807 (2011).

[27] R. Dovesi, R. Orlando, A. Erba, C. M. Zicovich-Wilson, B. Civalleri, S. Casassa, L. Maschio, M. Ferrabone, M. De La Pierre, P. D'Arco *et al.*, CRYSTAL14: A program for the *ab initio* investigation of crystalline solids, Int. J. Quantum Chem. **114**, 1287 (2014).

[28] P. Hohenberg and W. Kohn, Inhomogeneous electron gas, Phys. Rev. **136**, B864 (1964).

[29] H. J. Monkhorst and J. D. Pack, Special points for Brillouin-zone integrations, Phys. Rev.B **13**, 5188 (1976).

[30] T. Bredow, P. Heitjans, and M. Wilkening, Electric field gradient calculations for Li_x Ti S_2 and comparison with ^{7}Li NMR results, Phys. Rev.B **70**, 115111 (2004).

[31] S. Piskunov, E. Heifets, Eglitis, and R. I. Borstel, Bulk properties and electronic structure of $SrTiO_3$, $BaTiO_3$, $PbTiO_3$ perovskites: An *ab initio* HF/DFT study Comput. Mater. Sci. **29**, 165 (2004).

[32] M. Towler, Crystal resources page, http://www.tcm.phy.cam.ac.uk/~mdt26/crystal.html (accessed: June 2011).

[33] X. Y. Cao and M. Dolg, Segmented contraction scheme for small-core lanthanide pseudopotential basis sets, J. Mol. Struct. Theochem. **581**, 139 (2002).

[34] D. Li, S. Gariglio, C. Cancellieri, A. Fte, D. Stornaiuolo, and J.-M. Triscone, Fabricating superconducting interfaces between artificially grown $LaAlO_3$ and $SrTiO_3$ thin films, APL Mater. **2**, 012102 (2014); C. Cancellieri, N. Reyren, S. Gariglio, A. D. Caviglia, A. Fte, and J.-M. Triscone, Influence of the growth conditions on the $LaAlO_3/SrTiO_3$ interface electronic properties, Europhys. Lett. **91**, 17004 (2010).

[35] V. N. Strocov, X. Wang, M. Shi, M. Kobayashi, J. Krempasky, C. Hess, T. Schmitt, and L. Patthey, Soft-x-Ray ARPES facility at the ADRESS beamline of the SLS: Concepts, technical realisation and scientific applications, J. Synchrotron Radiat. **21**, 32 (2014).

[36] M. P. Seah and W. A. Dench, Quantitative electron spectroscopy of surfaces: A standard data base for electron inelastic mean free paths in solids, Surf. Interface Anal. **1**, 2 (1979).

[37] A. Chikina, F. Lechermann, M.-A. Husanu, M. Caputo, C. Cancellieri, X. Wang, T. Schmitt, M. Radovic, and V. N. Strocov, Orbital ordering of the mobile and localized electrons at oxygen-deficient $LaAlO_3/SrTiO_3$ Interfaces, ACS Nano **12**, 7927 (2018).

[38] V. N. Strocov, C. Cancellieri, and A. S. Mishchenko, *Electrons and Polarons at Oxide Interfaces Explored by Soft-X-Ray ARPES*, Springer Series in Materials Science (Springer, Cham, 2016), Vol. 266.

[39] A. Filippetti, C. D. Pemmaraju, S. Sanvito, P. Delugas, D. Puggioni, and V. Fiorentini, Variational pseudo-self-interaction-corrected density functional approach to the *ab initio* description of correlated solids and molecules, Phys. Rev. B **84**, 195127 (2011).

[40] T. Archer, C. D. Pemmaraju, S. Sanvito, C. Franchini, J. He, A. Filippetti, P. Delugas, D. Puggioni, V. Fiorentini, R. Tiwari *et al.*, Exchange interactions and magnetic phases of transition metal oxides: Benchmarking advanced *ab initio* methods, Phys. Rev. B **84**, 115114 (2011).

[41] D. I. Bilc, R. Orlando, R. Shaltaf, G.-M. Rignanese, J. Íñiguez, and P. Ghosez, Hybrid exchange-correlation functional for accurate prediction of the electronic and structural properties of ferroelectric oxides, Phys. Rev. B **77**, 165107 (2008).

[42] C. Cancellieri, M. L. Reinle-Schmitt, M. Kobayashi, V. N. Strocov, P. R. Willmott, D. Fontaine, P. Ghosez, A. Filippetti, P. Delugas, and V. Fiorentini, Doping-dependent band structure of $LaAlO_3/SrTiO_3$ interfaces by soft x-ray polarization-controlled resonant angle-resolved photoemission, Phys. Rev. B **89**, 121412 (2014).

[43] C. Cancellieri, A. S. Mishchenko, U. Aschauer, A. Filippetti, C. Faber, O. S. Barišić, V. A. Rogalev, T. Schmitt, N. Nagaosa, and V. N. Strocov, Polaronic metal state at the $LaAlO_3/SrTiO_3$ interface, Nat. Commun. **7**, 10386 (2016).

[44] V. N. Strocov, Photoemission response of 2D electron states, J. Electron Spectrosc. Relat. Phenom. **229**, 100 (2018).

[45] N. C. Plumb, M. Kobayashi, M. Salluzzo, E. Razzoli, C. E. Matt, V. N. Strocov, K. J. Zhou, M. Shi, J. Mesot, T. Schmitt *et al.*, Evolution of the $SrTiO_3$ surface electronic state as a function of $LaAlO_3$ overlayer thickness, Appl. Surf. Sci. **412**, 271 (2017).

[46] Z. Wang, S. McKeown Walker, A. Tamai, Y. Wang, Z. Ristic, F. Y. Bruno, A. de la Torre, S. Riccò, N. C. Plumb, M. Shi *et al.*, Tailoring the nature and strength of electron–phonon interactions in the $SrTiO_3$ (001) 2D electron liquid, Nat. Mater. **15**, 835 (2016).

[47] C. Chen, J. Avila, E. Frantzeskakis, A. Levy, and M. C. Asensio, Observation of a two-dimensional liquid of Fröhlich polarons at the bare $SrTiO_3$ surface, Nat. Commun. **6**, 8585 (2015).

[48] Z. Wang, Z. Zhong, S. McKeown Walker, Z. Ristic, J.-Z. Ma, F. Y. Bruno, S. Riccò, G. Sangiovanni, G. Eres, N. C. Plumb *et al.*, Atomically precise lateral modulation of a two-dimensional electron liquid in anatase TiO_2 thin films, Nano Lett. **17**, 2561 (2017).

[49] E. Maniv, M. Ben Shalom, A. Ron, M. Mograbi, A. Palevski, M. Goldstein, and Y. Dagan, Strong correlations elucidate the electronic structure and phase diagram of $LaAlO_3/SrTiO_3$ interface, Nat. Commun. **6**, 8239 (2015).

[50] A. E. M. Smink, J. C. de Boer, M. P. Stehno, A. Brinkman, W. G. van der Wiel, and H. Hilgenkamp, Gate-Tunable Band Structure of the $LaAlO_3-SrTiO_3$ Interface, Phys. Rev. Lett. **118**, 106401 (2017).

[51] A. E. M. Smink, M. P. Stehno, J. C. de Boer, A. Brinkman, W. G. van der Wiel, and H. Hilgenkamp, Correlation between superconductivity, band filling, and electron confinement at the $LaAlO_3/SrTiO_3$ interface, Phys. Rev. B **97**, 245113 (2018).